1

2

Nanosilver Targets the Bacterial Cell Envelope: The Link with Generation of Reactive Oxygen Radicals

5

6 [#]C. Gunawan[1,2,]*, [#]M.B. Faiz[2], R. Mann[1], S.R.S. Ting[3], G.A. Sotiriou[4], C.P. Marquis[5],

7 R. Amal[2]

8 [#]*Equal author contribution*

9

10 [1]ithree institute, University of Technology Sydney, NSW 2007, Australia

11 [2]School of Chemical Engineering, University of New South Wales, Sydney, NSW 2052,
12 Australia

13 [3]Centre for Health Technologies, University of Technology Sydney, NSW 2007, Australia

14 [4]Department of Microbiology, Tumor and Cell Biology, Karolinska Institutet, Stockholm,
15 Sweden

16 [5]School of Biotechnology and Biomolecular Sciences, University of New South Wales,
17 Sydney, NSW 2052, Australia
18
19
20
21
22
23
24
25
26
27

28 *Corresponding author at the ithree institute, University of Technology Sydney, NSW 2007,
29 Australia. Tel.: +61 295148203. E-mail address: Cindy.Gunawan@uts.edu.au

ABSTRACT

The work describes the interactions of nanosilver (NAg) with bacterial cell envelope components at molecular level and how this associates with the reactive oxygen species (ROS)-mediated toxicity of the nanoparticle. Major structural changes were detected in cell envelope biomolecules as a result of damages in functional moieties, such as the saccharides, amides and phosphodiesters. NAg exposure disintegrates the glycan backbone in the major cell wall component peptidoglycan, causes complete breakdown of lipoteichoic acid as well as disrupting the phosphate-amine and fatty acid groups in phosphatidylethanolamine, a membrane phospholipid. Consistent with oxidative attacks, we propose that the observed cell envelope damages are inflicted, at least in part, by the reactive oxygen radicals being generated by the nanoparticle during its leaching process, abiotically, without cells. The cell envelope targeting, especially those on the inner membrane phospholipid, is likely to then trigger the rapid generation of lethal levels of cellular superoxide ($O_2^{\bullet-}$) and hydroxyl ($OH^{\bullet}$) radicals herein seen with a model bacterium. The present study provides a better understanding of the antibacterial mechanisms of NAg, whereby ROS generation could be both the cause and consequence of the toxicity, associated with the initial cell envelope targeting by the nanoparticle.

Keywords: silver nanoparticle, cell envelope, peptidoglycan, lipopolysaccharide, lipoteichoic acid, phospholipid, reactive oxygen radicals, toxicity

INTRODUCTION

Advances in nanoparticle design and engineering have enabled incorporation of silver nanoparticle (NAg), an ultrafine less than 100 nm metallic or oxide silver in medical devices, such as in wound dressings and catheters, to prevent or treat established infections. The broad spectrum antimicrobial particle has also been increasingly found in consumer products and appliances, from clothing and water filters, to baby toys and refrigerators.[1,2] In line with the commercialization, our understanding of the nanoparticle's modes of antimicrobial action has indeed started to mature with many scholarly studies revealing the complex toxicity paradigms. In contrast to the single antimicrobial source of ionic silver (most commonly in the form of soluble silver salt, such as $AgNO_3$), studies have found that both the soluble silver species that leaches out from NAg upon contact with aqueous environments, and the solid silver particulates that remain after leaching, contribute to the overall toxicity.[3-6] The extent of leaching is affected by the nanoparticle's physicochemical characteristics, including its size.[6] Though still a controversy, such size-dependent variation in the leaching behaviour is thought to be one of the major factors for the generally less potent micron-sized silver particles when compared to their nano-sized counterparts.[7,8]

NAg exposure has been known to destabilize enzymes and structural proteins in bacteria due to the high affinity of the leached Ag(I) ion for amine and sulfur groups that are present in amino acid side chains.[9,10] Studies have also observed DNA damage following exposure to the nanoparticle.[11,12] A more detailed knowledge on NAg reactivity however, is required, in particular on the initial triggers of the antibacterial actions. Reports have documented 'physical' electron microscopy evidence of cell surface damage in bacteria and quite recently, a report on the disordered states of cell surface moieties in NAg-bacterial samples.[13,14] Yet, only little is known on the nature of this cell surface disruption and equally important, its potential link to the cellular oxidative stress, which ultimately result in the growth inhibition and cell death effects.[3,5,15] Despite being seen as one of the major toxicity paradigms of NAg, inquiries are still being raised in regard to the generation mechanisms of these reactive oxygen species as well as their toxic implications.

Our work investigated NAg targeting of the bacterial cell envelope components, seeking to identify structural changes at a molecular level. For this purpose, we used the attenuated total reflectance – Fourier-transform infrared (ATR-FTIR) spectroscopy

91 technique, which allows detection of specific chemical bond changes without the
92 potentially destructive prior treatments of the biomolecules.[16,17] The study also
93 examined the generation of oxygen radicals by the nanoparticle, in the absence of
94 cells, and intracellularly, with a model bacterium. Altogether, the analyses not only give
95 insights into the cause and forms of the cell envelope attack, but also the process of
96 oxygen radical generation inside the cells. Unlike molecular oxygen (O_2), oxygen
97 radical species, such as singlet oxygen ($O_2(^1\Delta_g)$), superoxide ($O_2^{\bullet-}$) and hydroxyl ($OH^\bullet$)
98 radicals, have an oxygen atom with an unpaired electron, rendering them unstable and
99 chemically reactive. The detection and identification of cellular ROS is therefore
100 challenging due to the very short nano to micro seconds half-lives of oxygen
101 radicals.[18,19] To overcome this, we used the electron paramagnetic resonance (EPR)
102 spectroscopy coupled with a cell-permeable spin probing technique. The non-toxic spin
103 probe is sensitive to the presence of cellular oxygen radicals, being oxidized to form
104 the EPR-detectable nitroxides with half-life of several hours, even in biological
105 environments.[20,21] The work presented herein, deciphers the molecular intricacies
106 surrounding the NAg-inflicted damage on the bacterial cell envelope and its association
107 to the ROS generation.

RESULTS AND DISCUSSION

109   **NAg effects on peptidoglycan**. Peptidoglycan (PGN) is a mesh-like polymer
110 moiety that is present in the cell wall structure of both Gram-positive and Gram-negative
111 bacteria (**Scheme 1**). In Gram-positive bacteria, PGN forms the outermost layer of their
112 cell wall, while in Gram-negative bacteria, it is present in the periplasmic space,
113 between the outer and inner cytoplasmic membranes. Structurally, PGN is an
114 alternating co-polymer of two sugar derivatives, N-acetylglucosamine (NAG) and N-
115 acetylmuramic acid (NAM), covalently linked by the β-(1,4)-glycosidic bond (**Fig 1B**).
116 Attached to NAM is a four-to-five amino acid long peptide chain, depending on the type
117 of bacteria. The sugar and amino acid constituents form a repeating structure, referred
118 to as the glycan strand. The ATR-FTIR spectra of PGN are shown in **Fig 1A** (black
119 spectra) with the band assignments summarized in **Table 1**. The presence of NAG and
120 NAM sugar units correspond to the occurrence of IR spectral peaks at 1158 cm^{-1} (C-O
121 stretching vibration of saccharides), 1062 cm^{-1} (C-O and C-C stretching vibration of
122 saccharides) and 984 cm^{-1} (COH bending and C-O stretching vibration of saccharides).
123 The presence of the peptide chain corresponds to the amide bands at ~3266 cm^{-1}
124 (amide A), ~3067 cm^{-1} (amide B), 1624 cm^{-1} (amide I) and 1531 cm^{-1} (amide II),

125 although these may also correspond to amide groups that are present in the sugars.
126 Note that the C-H bond peaks at 2962, 2928 and 2875 cm^{-1} refer to the hydrocarbon
127 moieties in both the sugar and peptide chain units. The glycan strands are cross-linked
128 *via* an interbridge peptide bond or glycine group (depending on the type of bacteria),
129 connecting peptide chains from the different strands to form the overall PGN mesh-like
130 structure (**Fig 1B**). The NAG-NAM glycosidic bond together with the cross-linking of the
131 glycan strands in PGN provides the bacterial cell wall with rigidity in longitudinal and
132 transverse direction, respectively.
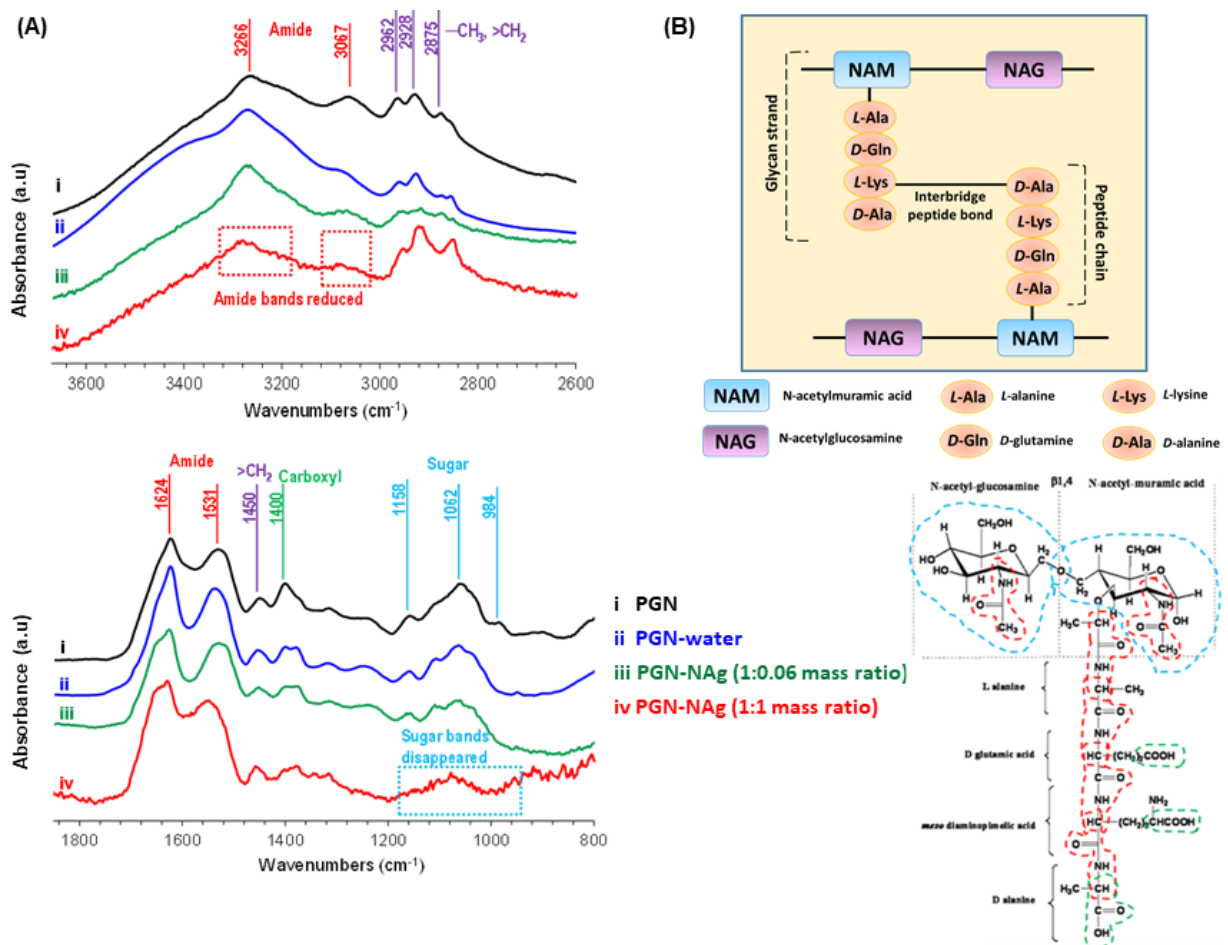
133

134 **Figure 1. Peptidoglycan (PGN) exposure to NAg.** (**A**) ATR-FTIR spectra (3670 – 2600 cm^{-1}
135 and 1850 – 800 cm^{-1} wavenumber) of PGN, PGN-water (to account for the potential effect of
136 the aqueous exposure environment) and NAg-treated PGN. The spectra shown is a
137 representative of two independent experiments. Refer to **Fig S1** for the replicate spectra of this
138 experiment. (**B**) Structural representation of PGN. The colours of the functional groups in (B)
139 match the colours of assigned bands in (A). The PGN is from *B. subtilis*, with *L*-alanine, *D*-
140 glutamic acid, diaminopimelic acid and *D*-alanine composing the peptide chain.

141   Upon exposure to NAg, changes in the PGN spectra were observed (**Fig 1A**,
142 summarized in **Table 2** are the corresponding changes in the molecular structure). We

143 detected significant decrease of the ~3266 cm^{-1} amide A and ~3067 cm^{-1} amide B
144 bands in the nanoparticle treated samples when compared to those of the PGN-only
145 and PGN-water samples, indicating damage on the amide groups. Based on a circular
146 dichroism spectroscopy work by Mirzajani et al., it is thought that these amide groups
147 are those of the peptide chain, with the NAg exposure altering the secondary structure
148 of the chain.[22] We next observed the disappearance of the 1158, 1062 and 984 cm^{-1}
149 saccharide bands that form the NAG and NAM sugars, indicating disintegration of the
150 glycan strands. This is in agreement with the reported release of muramic acid in
151 bacterial samples following exposure to NAg.[22] This disruption in PGN structure could
152 be one of the causes for the formation of 'pits' in the cell wall that are frequently seen
153 in electron microscopy images of NAg-treated Gram-positive and Gram-negative
154 bacteria.[14,22-24] PGN is designed to withstand the relatively high osmotic pressure (~20
155 atmosphere) of the cytoplasm[25] and impairment to its structure could result in cell lysis
156 due to disturbance of the cytoplasm's osmotic balance.[26,27]

157   **NAg effects on lipopolysaccharide.** The amphiphilic polysaccharide (LPS) is a
158 major component of the outer membrane of Gram-negative bacteria (**Scheme 1**). While
159 the exact molecular structures of LPS vary among different species of bacteria, the
160 main components are in general conserved, being composed of the lipid A, core region
161 and O-antigen (**Fig. 2B**). Chains of fatty acids in lipid A are connected to the core region
162 through amine groups of glucosamine phosphate moieties. Both the core region and
163 O-antigen are polysaccharides. The hydrophobic lipid A is anchored to the inner leaflet
164 of the outer membrane, while the hydrophilic O-antigen is exposed to the external
165 environment.[28-30] The presence of fatty acids in lipid A correspond to the occurrence of
166 spectral peaks at 2955, 2919, 2851 cm^{-1} (C-H asymmetric stretching of CH$_3$, C-H
167 asymmetric and symmetric stretching of CH$_2$ in fatty acids, respectively), 1734 cm^{-1}
168 (C=O stretching vibration of ester) and 1382, 1346, 1225 cm^{-1} (CH$_3$ umbrella symmetric
169 bending vibration in the lipids) (**Fig 2A** (black spectra), **Table 1**). The presence of
170 glucosamine phosphates in lipid A correspond to the bands at 3263, 3088, 1645, 1560,
171 975 cm^{-1} (amide A, amide B, amide I, amide II and C-N asymmetric stretching vibration,
172 respectively), saccharide bands at 1136 cm^{-1} (C-O ring stretching), 1075, 1025 cm^{-1}
173 (C-O stretching, C-C stretching and COH bending), and 1061 cm^{-1} (C-O stretching, C-
174 C stretching), as well as phosphate band at 1208 cm^{-1} (P=O asymmetric stretching).
175 The saccharide bands also correspond to those present in the core region and O-
176 antigen.

Table 1. Assignment of the ATR-FTIR spectra of the bacterial cell envelope components

Peptidoglycan [16,31,32,33]		Lipopolysaccharide [16,28,32,34]		Lipoteichoic acid [16,28,32,33]		Phosphatidylethanolamine [16,28,33]	
cm⁻¹		cm⁻¹		cm⁻¹		cm⁻¹	
~3266	Amide A	3263	Amide A	3211	Amide A		
~3067	Amide B	3088	Amide B				
2962	v_a(CH$_3$)	2955	v_a(CH$_3$)			2955	v_a(CH$_3$)
2928	v_a(CH$_2$)	2919	v_a(CH$_2$)	2924	v_a(CH$_2$)	2917	v_a(CH$_2$)
2875	v_s(CH$_3$)					2871	v_s(CH$_3$)
		2851	v_s(CH$_2$)	2854	v_s(CH$_2$)	2850	v_s(CH$_2$)
		1734	v(C=O) of ester	1741	v(C=O) of ester	1732	v(C=O) of ester
1624	Amide I	1645	Amide I	1638	Amine I (asymmetrical amine)	1640	Amine I
1531	Amide II	1560	Amide II	1554	Amine II (symmetrical amine)	1579	Carboxylate stretching
				1456	δ_a (CH$_3$)	1467	δ(CH$_2$) scissor in lipids
1400	v_s(C=O) of COO⁻	1406	v_s(COO⁻)			1417	δ(α−CH$_2$) scissoring mode attached to CO or PO
		1382	δ_s(CH$_3$) umbrella in lipids	1375	δ_s(CH$_3$) umbrella in lipids	1379	δ_s(CH$_3$) umbrella in lipids
		1346		1337		1342	
		1225				1294	
		1287	Amide III				
						1247	v_a(P=O) of PO$_2^-$ (phosphodiester)
		1208	v_a(P=O) of PO$_2^-$	1208	v_a(P=O) of PO$_2^-$ (phosphodiester)	1218	
1158	v(C-O) of saccharides	1136	v(C-O) ring of saccharides			1177	v_{as} (C-O-C) in esters
		1075	v(C-O), v(C-C), δ(COH) of saccharides	1009	v(C-O), v(C-C), δ(COH) of saccharides	1083	v_s(P=O) of (PO$_2^-$) of phosphodiester
		1025					
1062	v(C-O), v(C-C) of ring of saccharides	1061	v(C-O), v(C-C) of ring of saccharides				
984	δ(COH),v(C-O) of saccharides	975	v_a(C-N)	955	Ring of saccharides		
						757	v_s (P-O-C)

177

178

179　　　　Unlike those seen with the PGN, we only detected mild effects of NAg exposure on

180　　LPS, with no major spectral changes (relative to the LPS-only and LPS-water samples).

181　　The 2955 cm^{-1} CH$_3$ peak of the fatty acid chain was more intense (**Fig 2A,** black arrow,

182　　**Table 2**). The saccharide peak at 1075 cm^{-1} also slightly shifted to a lower wavenumber

183　　(2-4 cm^{-1}, blue arrows in **Fig 2A**), indicating weakening of the C-O bonds in the

184　　saccharides. This bond weakening is thought to associate with the reported hydrogen

185　　bonding of LPS with NAg, most likely involving the hydrophilic O-antigen.[28,35,36]

186　　However, it is possible that this O-antigen-nanoparticle interaction does not significantly

187　　contribute to the overall toxicity of NAg. Gram-negative bacteria have been known to

188　　use their LPS polysaccharide elements, including those of the O-antigen as general

189　　mechanisms to interact and attach on solid surfaces in the environment.[28,37]

190　　Regardless, this hydrogen bonding could be one of the initial interactions of the

191　　bacterium with NAg.
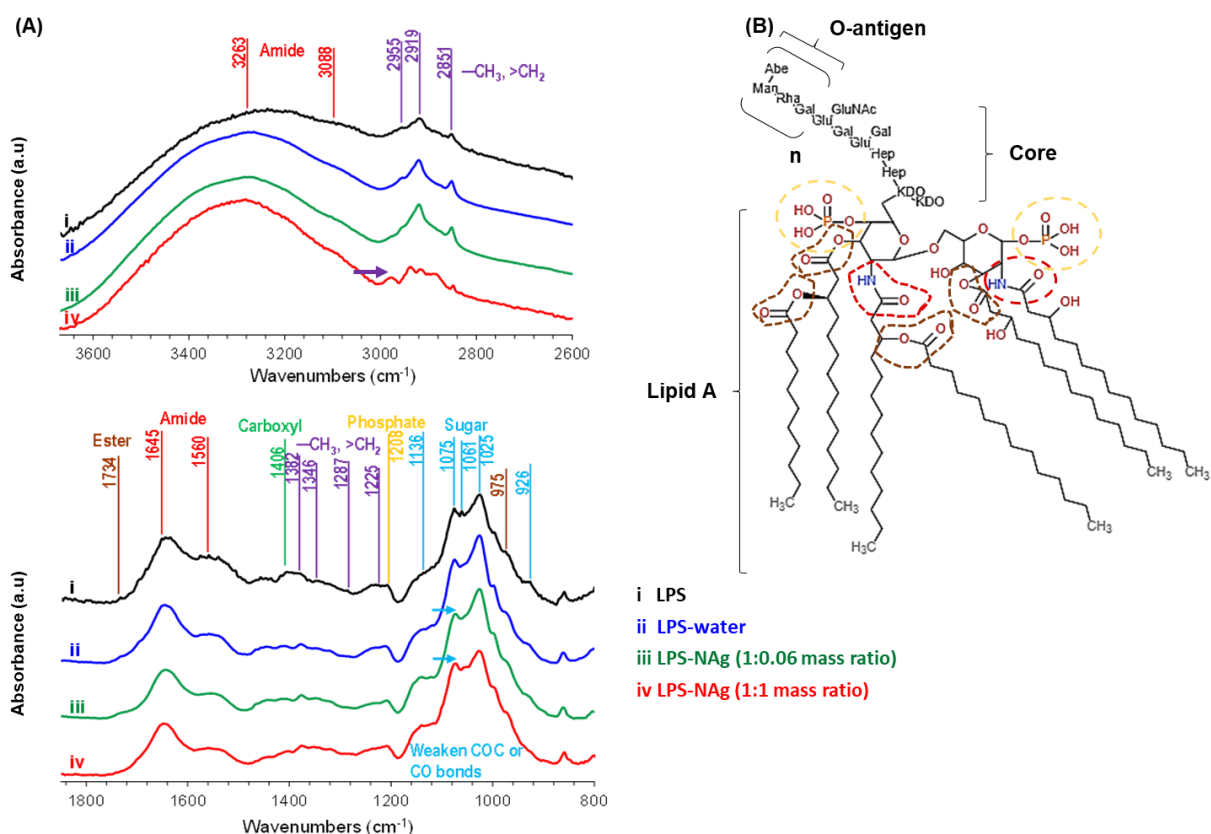
192

193　　**Figure 2. Lipopolysaccharide (LPS) exposure to NAg.** (**A**) ATR-FTIR spectra (3670 – 2600

194　　cm^{-1} and 1850 – 800 cm^{-1} wavenumber) of LPS, LPS-water and NAg-treated LPS. Refer to

195　　**Figure S2** for the replicate spectra of this experiment. (**B**) Structural representation of LPS.

196　　The colours of the functional groups in (B) match the colours of assigned bands in (A). The

197　　LPS is from *E. coli.*

198   **NAg effects on lipoteichoic acid**. Lipoteichoic acid (LTA) is a cell wall molecule
199   in Gram-positive bacteria (**Scheme 1**). LTA is an amphiphilic molecule, composed of
200   the hydrophilic glycerophosphate moiety that covalently binds to the hydrophobic
201   glycolipid *via* a phosphodiester bond (**Fig 3B**).[28,29] The glycerophosphate unit is made
202   of a phosphodiester 'backbone', which corresponds to the spectral peak at 1208 cm^{-1},
203   assigned to P=O asymmetric stretching vibration of PO$_2^-$ (**Fig 3A** (black spectra), **Table
204   1**). Attached to the phosphodiester backbone are *D*-alanyl and/or glycosyl 'side
205   branches' to varying degrees, depending on the species of the bacteria (*D*-alanine and
206   acetylglucosamine in *B. subtilis*). The presence of the *D*-alanine branch corresponds to
207   the spectral bands at 1638 and 1554 cm^{-1} (due to deformation of RNH$_3^+$ or RNH$_2$) and
208   1741 cm^{-1} (C=O stretching vibration of ester), while the presence of acetylglucosamine
209   corresponds to the bands at 3211 cm^{-1} (amide A), 1009 cm^{-1} (C-O stretching, C-C
210   stretching and COH bending of saccharides) and 955 cm^{-1} (ring of saccharides). Note
211   that the saccharide bands could also correspond to the presence of oligosaccharides
212   in the glycolipid. The glycolipid commonly consists of oligosaccharides of *D*-glucose
213   with glycosidically bound 1,2-diacyl-*sn*-glycerol. The presence of lipid corresponds to
214   the appearance of CH$_3$ bending modes of lipid at 1456, 1375, and 1337 cm^{-1} as well as
215   the 1741 cm^{-1} ester band.

216   The nanoparticle exposure inflicted significant damage on the LTA molecule. First,
217   for the glycerophosphate unit, we observed the disappearance of the 1208 cm^{-1} P=O
218   peak of the phosphodiester backbone (relative to the LTA-only and LTA-water samples)
219   (**Fig 3A**, **Table 2**), possibly due to the formation of P-O-NAg *via* ligand exchange.[28,36,38]
220   We also observed the disappearance of the 1009 cm^{-1} saccharide and the 955 cm^{-1}
221   ring of saccharide bands, indicating disintegration of the saccharide components in the
222   acetylglucosamine side branch, and also most likely, those in the glycolipid. The 3211
223   cm^{-1} amide A band of the acetylglucosamine branch also disappeared. Damage to the
224   *D*-alanine branch was also seen, with the disappearance of the 1638 and 1554 cm^{-1}
225   amine peaks. Finally, we observed the disappearance of the 1741 cm^{-1} C=O band of
226   ester, which could refer to those present in both the *D*-alanine branch and the 1,2-
227   diacyl-*sn*-glycerol part of the glycolipid. Note that there was an appearance of a new
228   peak at ~1500 cm^{-1}, which could be assigned to any remaining presence of CH$_2$
229   hydrocarbon. To date, there are still controversies surrounding the exact functions of
230   LTA, the molecule however, is thought to be essential for bacterial growth and as
231   building blocks for metabolism.[39] The observed complete breakdown of LTA is

232　therefore likely to cause growth inhibition, a known effects of NAg on Gram-positive
233　bacteria.[3,40]
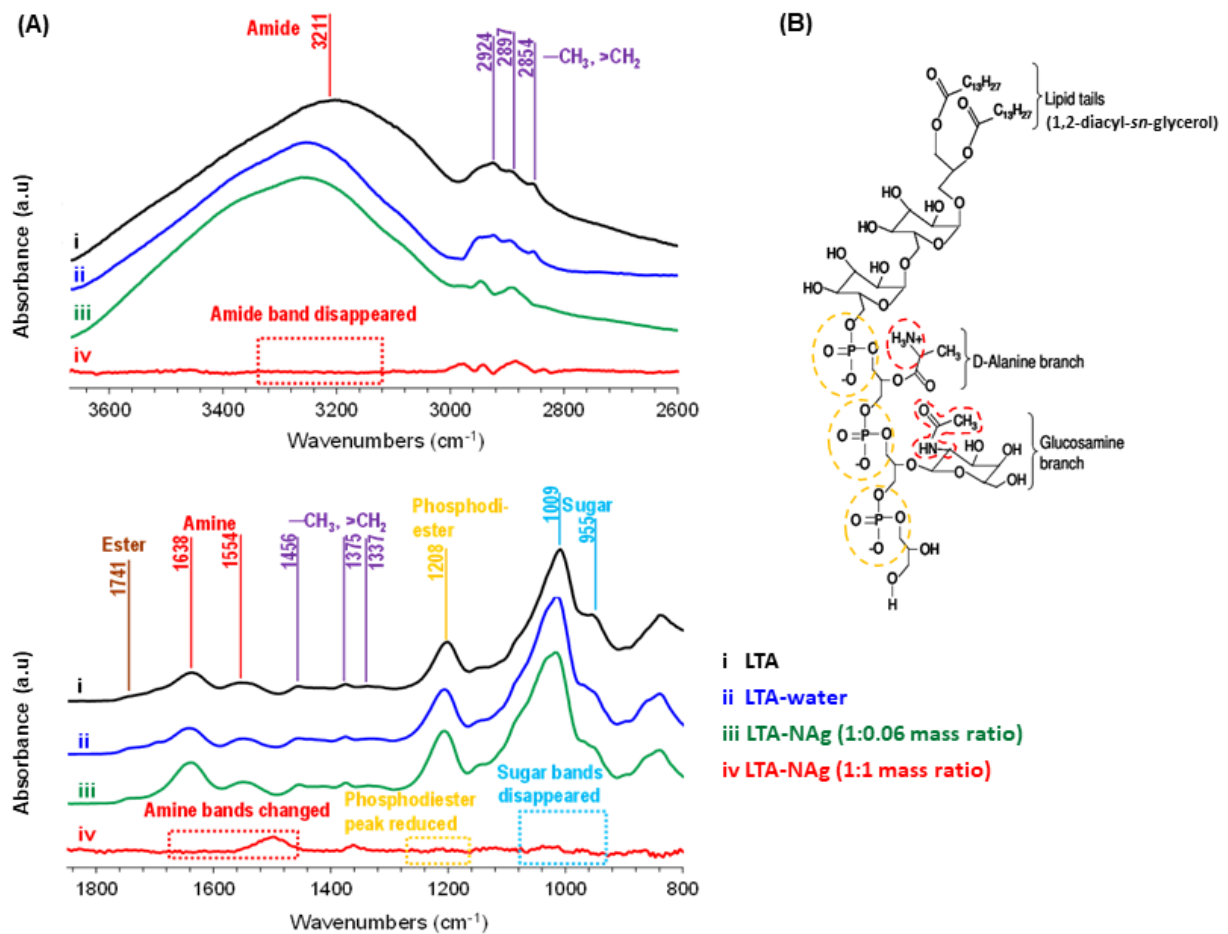
Figure 3. Lipoteichoic acid (LTA) exposure to NAg. (A) ATR-FTIR spectra (3670 – 2600 cm^{-1} and 1850 – 800 cm^{-1} wavenumber) of LTA, LTA-water, NAg-treated LTA. Refer to **Fig S3** for the replicate spectra of this experiment. **(B)** Structural representation of LTA (adapted from Jiang et al. 2010) [28]. The colours of the functional groups in (B) match the colours of assigned bands in (A). The LTA is from *B. subtilis* with *D*-alanine and acetylglucosamine as side branches.

NAg effects on phosphatidylethanolamine. Phosphatidylethanolamine (PE) is one of the major phospholipids forming the general structure of the cytoplasmic (inner) membrane of both Gram-positive and Gram-negative bacteria, and the outer membrane of Gram-negative bacteria (**Scheme 1**). PE is an amphiphilic molecule with hydrophilic phosphate-amine 'head' and hydrophobic fatty acid 'tail' components (**Fig 4B**).[29,30] The presence of the phosphate head corresponds to the appearance of spectral peaks at 1247 (at 1218 cm^{-1} too) and 1083 cm^{-1}, which are assigned to P=O asymmetric and symmetric stretching of PO$_2^-$ of phosphodiester, respectively, as well

249   as at 757 cm^{-1} to P-O-C symmetric stretching vibration, while the amine moiety

250   corresponds to spectral bands at 1640 cm^{-1} (deformation of RNH^{3+} or RNH$_2$) (**Fig 4A**

251   (black spectra), **Table 1**). The presence of the fatty acid tail corresponds to the spectral

252   peaks at 1732 and 1177 cm^{-1}, which are assigned to C=O and C-O-C stretching

253   vibration of ester, respectively, as well as bands at ~1500-1300 cm^{-1}, which mainly

254   associate with the C-H deformation of alkyl chains. This amphiphilic character of PE

255   renders the membranes capable to act as a selective permeability barriers for the

256   bacteria.[41]

257   Based on the spectral changes (**Fig 4A, Table 2**), NAg is indicated to target the

258   phosphate head of PE. A substantial reduction of the 1218 and 1083 cm^{-1} P=O peaks

259   of phosphodiester and the 757 cm^{-1} (P-O-C) bands were detected (relative to the PE-

260   only and PE-water samples), and not surprisingly, the disappearance of the 1640 cm^{-1}

261   amine band, which could again result from the P-O-NAg.[28,30] Damage to the phosphate

262   head is thought to have caused the highly disordered states of the fatty acid tail, herein

263   indicated by the appearance of multiple new peaks at the ~1370-1300 cm^{-1} alkyl chain

264   region, as well as, the weakening of a peak at 3010 cm^{-1}, the latter possibly refers to

265   the oxidation of C=C bond. (**Fig 4A**).[28,30] The disruptions in both the hydrophilic and

266   hydrophobic components of PE suggest loss of its amphiphilic character, which could

267   cause the membranes to lose their selective barrier function, leading to leakage.

268   Studies have observed outflows of sugars and proteins from the cytoplasm following

269   exposure of both Gram-positive and Gram-negative bacteria to NAg.[23,42] The

270   phospholipid targeting are also consistent with the membrane disarrays seen in NAg-

271   treated bacterial samples, both Gram-positives and Gram-negatives.[3,5,14,23,24]

272
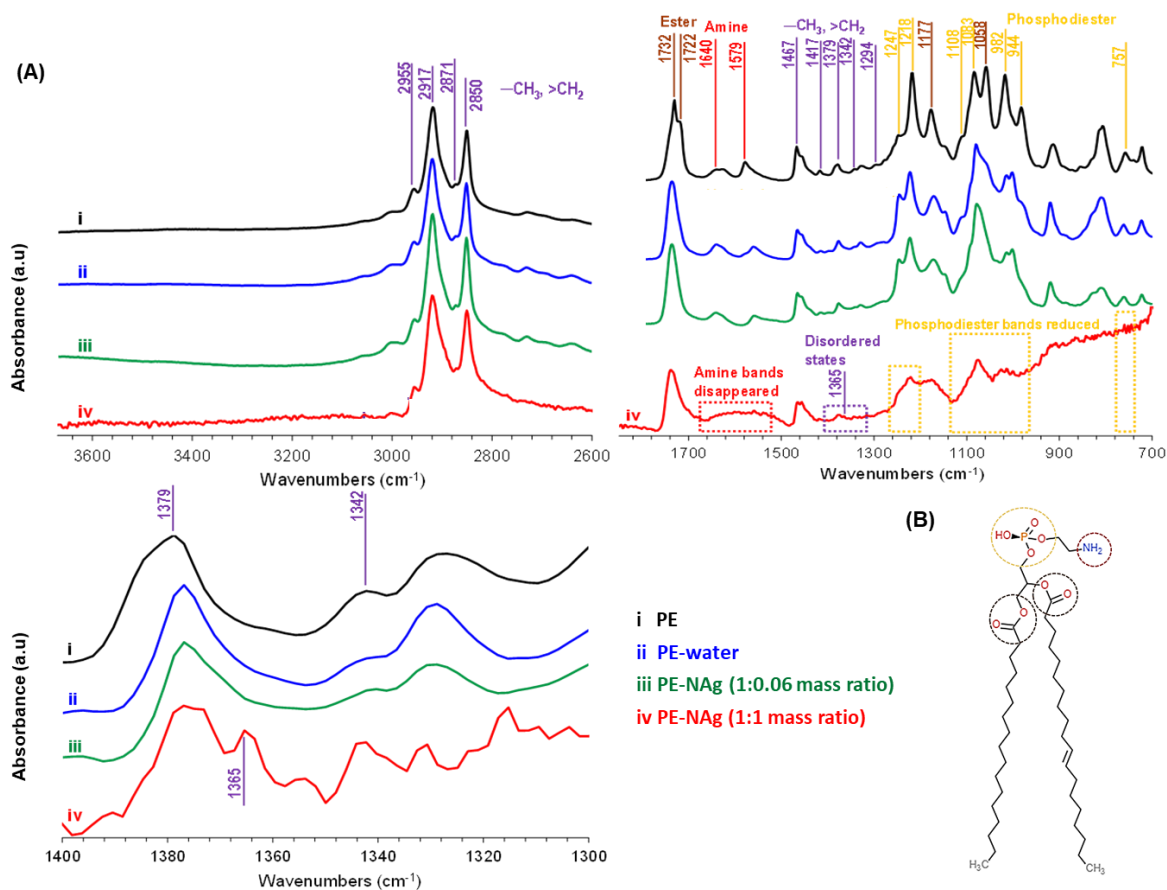
Figure 4. Phosphatidylethanolamine (PE) exposure to NAg. (A) ATR-FTIR spectra (3670 – 2600 cm^{-1} and 1850 – 700 cm^{-1} wavenumber) of PE, PE-water, NAg-treated PE, also shown is a zoomed-in spectra at 1400 – 1300 cm^{-1} that correspond to the C-H deformation region. Refer to **Fig S4** for the replicate spectra of this experiment. (B) Structural representation of PE. The colours of the functional groups in (B) match the colours of assigned bands in (A). The PE is from *E. coli*.

279

Table 2. NAg-induced structural changes in cell envelope molecules

Wavenumber (cm^{-1})	Spectral changes	Changes in molecular structure
Peptidoglycan		
~3266, ~3067 (1:1 PGN to NAg mass ratio)	Less intense amide A and amide B bands	Modification of the amide groups of PGN, possibly the peptide chain[22]
1158, 1062, 984 (1:1)	Disappearance of saccharide bands of NAG and NAM moieties	Disintegration of glycan strands
Lipopolysaccharide		
2955 (1:1)	More intense CH$_3$ peak	Unclear changes in the fatty acid chain
1075 (1:0.06, 1:1)	Shift of saccharide peak to lower wavenumber	Weakening of C-O bond in the saccharides
Lipoteichoic acid		
3211 (1:1)	Disappearance of amide A peak	Disintegration of the acetylglucosamine side branch
1741, 1638, 1554 (1:1)	Disappearance of C=O band of ester, amine peaks	Damages to the *D*-alanine side branch, the ester C=O bond could also refer to 1,2-diacyl-*sn*-glycerol unit of the glycolipid
1208 (1:1)	Disappearance of P=O peak	Disintegration of the phosphodiester backbone in the glycerophosphate unit
1009, 955 (1:1)	Disappearance of saccharide peaks	Disintegration of the saccharide groups in the glycolipid unit and the acetylglucosamine side branch
Phosphatidylethanolamine		
1247, 1218, 1083 (1:1) 757 (1:1) 1640 (1:1)	Less intense P=O peak Less intense P-O-C band Disappearance of amine band	Disintegration of the phosphate-amine 'head' unit, including its phosphodiester groups
~1370 – 1300 (1:1) 3010 (1:1)	Appearance of multiple new peaks (C-H) Less intense peak, possibly due to C=C oxidation	Disordered state of the fatty acids 'tail' unit[28,30]

Up to this stage, we have seen how NAg exposure alters and even disintegrates cell envelope functional units. NAg targets the glycan strands and peptide chains in peptidoglycan, the outermost layer of Gram-positive bacteria, while a thinner version also present in the periplasmic space of Gram-negative bacteria (**Scheme 1**). The nanoparticle also attacks both the phosphate-amine head and fatty acid tail of the major membrane phospholipid, phosphatidylethanolamine. In the case of Gram-negative bacteria, the phospholipid targeting also applies to those composing the outer membrane, although the present work did not find any major structural changes in

289 lipopolysaccharide, a major component of Gram-negative outer membrane. NAg also
290 damages lipoteichoic acid in Gram-positive bacteria. These cell envelope damages
291 could be caused by oxidative attack. Nanoparticles of transition metals, including silver,
292 have been indicated to be capable of 'abiotic' reactive oxygen species (ROS)
293 generation, that is, in the absence of cells.[43] We next investigated the generation of
294 ROS induced by the nanoparticle, both in the absence of cells and inside cells, to gain
295 insights into the potential link between the cell envelope attack and the stimulation of
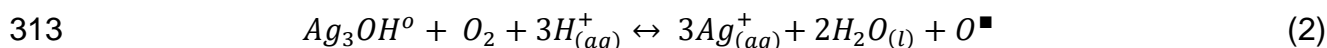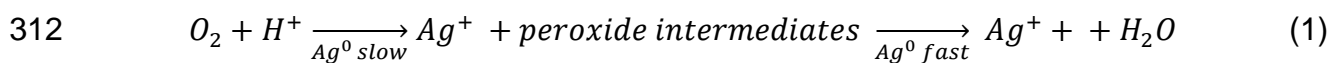296 cellular oxidative stress.
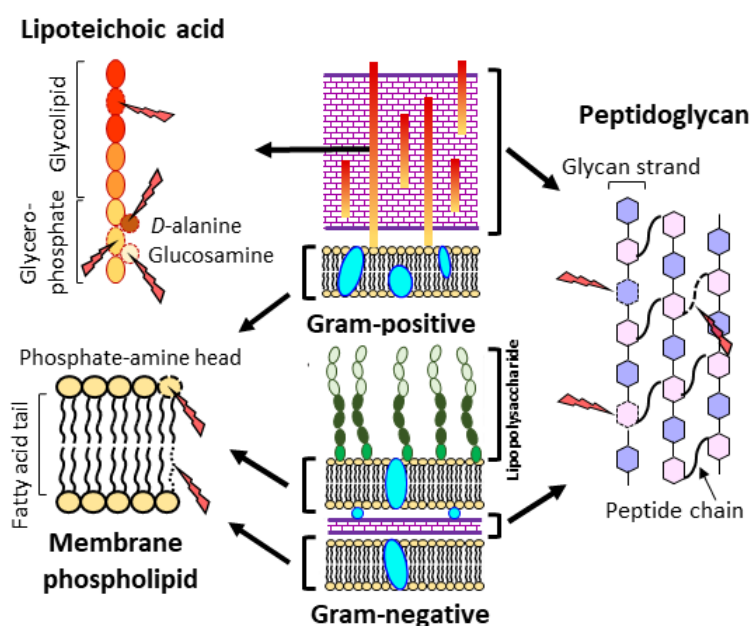
297

298 **Scheme 1.** NAg-inflicted structural damages on the Gram-positive and Gram-negative
299 bacteria cell envelope moieties.

300 **Generation of oxygen radicals and the link with cell envelope targeting.** Using
301 EPR spectroscopy, we detected ROS signals in the NAg-only systems, with no cells
302 (**Fig 5A**). These signals most likely correspond to the generation of superoxide radical
303 ($O_2^{\bullet-}$), to which the spin probe (CMH) has the highest affinity, as well as, possibly, to a
304 lesser extent, the presence of hydroxyl ($OH^{\bullet}$) and hydroperoxyl ($HO_2^{\bullet-}$) radicals, the
305 latter is the protonated form of $O_2^{\bullet-}$.[21,44] These oxygen radicals are thought to originate
306 from the leaching process of the nanoparticle.[3] Research inquiries have detected
307 oxygen radical intermediates during NAg dissolution (**Reaction 1**),[45,46] which has been
308 suggested to be thermodynamically more favourable than the direct reduction of O_2 to
309 water.[45,46] Studies have also suggested the formation of Ag_3OH^0 on the particulate

310   surface during leaching, which is then oxidized in the presence of O_2 to release Ag(I)

311   ions and oxygen radicals (from dissociation of O_2) (**Reaction 2**).[46]

$$O_2 + H^+ \xrightarrow[Ag^0\ slow]{} Ag^+ + peroxide\ intermediates \xrightarrow[Ag^0\ fast]{} Ag^+ + + H_2O \qquad (1)$$

$$Ag_3OH^o + O_2 + 3H^+_{(aq)} \leftrightarrow 3Ag^+_{(aq)} + 2H_2O_{(l)} + O^\blacksquare \qquad (2)$$
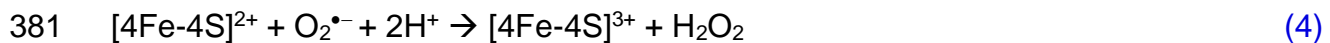
314   This abiotic ROS generation is most likely the source of the NAg attack on the cell

315   envelope components. Superoxide radical is capable of oxidative C-C bond cleaving

316   *via* hydrogen atom removal (abstraction) from O-H or C-H bonds.[47] This is consistent

317   with the observed disintegration of saccharide groups, those composing the glycan

318   strands in PGN as well as the glycolipid and *D*-acetylglucosamine side branch of LTA.

319   The C-C bond targeting could also be a factor in the detected disordered states of the

320   fatty acid tail of the phospholipid PE. The radical has also been shown to mediate acyl

321   carbon cleaving,[48] which is consistent with the observed damages on the PGN peptide

322   chain and also possibly, the *D*-alanine side branch of LTA. The cell envelope targeting

323   by NAg could also result from the activity of hydroxyl radical, which in fact, is the most

324   chemically reactive oxygen radical.[49] The radical can oxidize C=O of esters,[50] referring

325   to the nanoparticle attacks on those present in LTA, in its glycolipid (in the 1,2-diacyl-

326   *sn*-glycerol group) and *D*-alanine branch. OH$^\bullet$ can also damage amide bonds,[51] herein

327   seen with the peptide chain of PGN and the *D*-acetylglucosamine branch of LTA, as

328   well as cleaving phosphate esters,[52] like those found in the glycerophosphate unit of

329   LTA and the phosphate head of PE. Further, hydroperoxyl radical could trigger

330   oxidative chain reactions in polyunsaturated phospholipids, like PE.[49] Such damage to

331   the cell envelope structure could result in toxic silver species entering the bacteria.

332   Studies have indeed observed accumulation of NAg particulates in the inner membrane

333   of both Gram-positive and Gram-negative bacteria.[14,22,53]

334

335
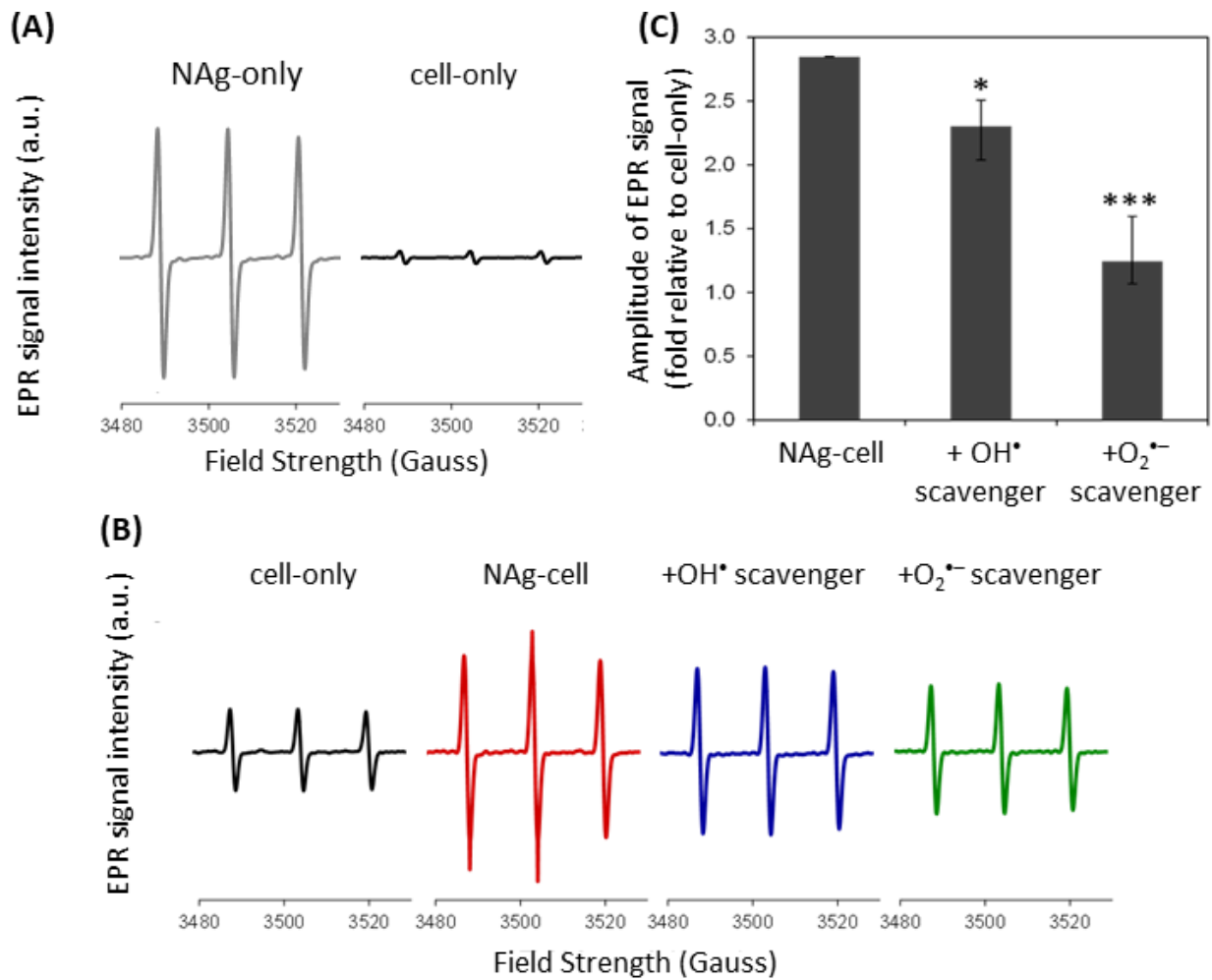
Figure 5. Reactive oxygen radical generation by NAg. (A) EPR spectra of ROS generated by NAg (no cells). **(B, C)** Cellular ROS detected in NAg-treated model bacterium (*B. subtilis*, 5 min exposure to the NAg MIC at 10 mg L^{-1} Ag.[3] The samples were also treated with superoxide ($O_2^{•-}$) and hydroxyl ($OH^•$) radical scavengers, SOD and DMTU, respectively. Also shown is the physiological cellular ROS levels in the cell-only samples (no silver). The spectra shown is a representative of three independent experiments. Refer to **Figure S5** for the replicate spectra of this experiment. In (C), the EPR signal amplitude was normalised to that of the cell-only control. Each data point is the average of three biological replicates (experiments with independent bacterial inocula and different antimicrobial preparations) with error bars representing the maximum and minimum. A one-way ANOVA (followed by Dunnett's posthoc) analysis was used to confirm the decrease of EPR signal in NAg-cell samples treated with the radical scavengers, with * and *** denoting p values of 0.0332 and 0.0002, respectively.

The NAg targeting of the cell envelope components, in particular the phospholipid, is most likely one of the key causes for the increased cellular ROS levels seen in many bacterial studies, including by our team.[3,5,13] These changes in the membrane constituents are consistent with the reported NAg-induced inhibition of the membrane-bound respiratory chain enzymes, which has been hypothesized to cause electrons leaking into the cytoplasm, in turn, reducing cytoplasmic molecular oxygen (O_2) to superoxide radicals.[23,24,54,55] Herein, we observed the elevated generation of superoxide radical in the model bacterium upon exposure to NAg (at the minimum inhibitory concentration, MIC of 10 mg Ag L^{-1} for the Gram-positive *B. subtilis*).[3] A ~3-fold higher cellular ROS EPR signals were detected relative to the cell-only samples (without silver) (**Fig 5B**). The addition of the $O_2^{\bullet-}$ radical scavenger enzyme, superoxide dismutase (SOD) reduced this ROS intensity by ~50% (**Fig 5C**), indicating that superoxide is one of the major oxygen radicals being generated in the NAg-treated cells. SOD catalyses the dismutation of superoxide radical to hydrogen peroxide (H_2O_2). In more detail, the enzyme catalyses an electron transfer from one $O_2^{\bullet-}$ to another $O_2^{\bullet-}$ (**Reaction 3**). The electron donor $O_2^{\bullet-}$ becomes a molecular oxygen (O_2), whilst the electron recipient $O_2^{\bullet-}$ combines with two protons generating H_2O_2.[29,56] In agreement, earlier studies have observed an increased expression of *sodA* gene that encodes a superoxide dismutase (MnSOD) subunit following exposure of the Gram-negative *E. coli* to NAg, indicating an increased presence of cellular $O_2^{\bullet-}$.[57] Note that the basal ROS detected in the cell-only samples refers to the physiological oxygen radicals being produced during aerobic metabolism, which involves a successive single-electron reduction of molecular oxygen.[29,58]

Apart from superoxide radical, our EPR studies also found presence of hydroxyl radical in the cells. A ~20% reduction in the cellular ROS signal intensity was detected when adding the $OH^{\bullet}$ scavenger dimethyl thiourea (DMTU) into the NAg exposure systems (**Fig 5C**). The hydroxyl radical generation is most likely to result from the attack of iron-sulfur clusters that are present in many enzymes by the $O_2^{\bullet-}$ radical.[58,59] These clusters, for example, are abundant in dehydratases, an enzyme family that has central roles in biosynthetic and catabolic pathways.[60,61] The oxidative attack releases the Fenton-active ferrous ions (Fe^{2+}) into the cytoplasm (**Reaction 4 and 5**), which react with cellular H_2O_2 to produce $OH^{\bullet}$ radical (Fenton reaction, **Reaction 6**).[54,61,62]

380      $O_2^{\bullet-} + O_2^{\bullet-} + 2H^+ \rightarrow O_2 + H_2O_2$ (3)

381      $[4Fe\text{-}4S]^{2+} + O_2^{\bullet-} + 2H^+ \rightarrow [4Fe\text{-}4S]^{3+} + H_2O_2$ (4)

382      $[4Fe\text{-}4S]^{3+} \rightarrow [3Fe\text{-}4S]^+ + Fe^{2+}$ (5)

383      $H_2O_2 + Fe^{2+} \rightarrow OH^{\bullet} + OH^- + Fe^{3+}$ (6)

384 $Fe^{3+} + O_2^{\bullet-} \rightarrow Fe^{2+} + O_2$ (7)

385   The cellular H_2O_2 could derive from the dismutation of $O_2^{\bullet-}$ by cellular SOD (**Reaction**

386   **3**), as well as, from the iron-sulfur clusters attack by $O_2^{\bullet-}$ (**Reaction 4**). Supporting the

387   Fenton-associated $OH^{\bullet}$ generation, Hwang et al. (2008) did not detect any increase in

388   the expression of *katG* gene in their *E. coli*-NAg exposure studies. The gene encodes

389   catalase, an H_2O_2 detoxification enzyme that functions as a complementary or second

390   tier antioxidant when there is a substantial presence of cellular H_2O_2, converting it to

391   O_2 and water.[57] The work therefore indicates minimal presence of cellular H_2O_2,

392   possibly feeding into the Fenton reaction. Further, other potential source for the Fenton-

393   active Fe^{2+}, apart from release from the iron-sulfur clusters, is the Haber-Weiss

394   reaction. In fact, the Fenton reaction is co-dependent with the latter, whereby ferric ions

395   (Fe^{3+}) are reduced by superoxide radical to generate Fe^{2+} (**Reaction 7**).[56,58,59] This

396   potential re-generation of Fe^{2+} could explain, at least in part, for the rapid $OH^{\bullet}$

397   production (detected within 5 min) in our NAg bacterial systems. Earlier bacterial

398   studies with Ag(I) ions (supplied as $AgNO_3$) reported a significant reduction in the

399   cellular $OH^{\bullet}$ levels upon addition of an iron quencher.[63] Ag(I) ions have been indicated

400   to also target the iron-sulfur clusters, releasing the Fenton-active Fe^{2+}.[59]

401   Superoxide and hydroxyl radicals have been shown to damage intracellular

402   molecules. Hydroxyl radical is well known for its lipid peroxidation activity, including on

403   glycolipids and phospholipids.[49] Initiated by the abstraction of an allylic hydrogen atom

404   by the radical, the peroxidation chain reaction modifies lipids into lipid

405   hydroperoxides.[64] The $OH^{\bullet}$ radical also targets base pairing and sugar moieties in DNA

406   and RNA.[12] Amino acids in proteins are also prone to oxidative attacks by the radicals,

407   in particular cysteine and methionine due to presence of the electron-rich sulfur atom

408   in their side chains.[9] As one-electron oxidants, $OH^{\bullet}$ and $O_2^{\bullet-}$, for example, can oxidize

409   the cysteine's thiol (-SH) to thiyl radicals ($RS^{\bullet}$) and the methionine's sulfur atom (in

410   thioether side chain) to sulfoxide. These covalent modifications can alter the protein

411   structure and in turn, inactivating the proteins.[9,65,66] This ROS targeting of biomolecules

412   is clearly a factor in the rapid killing seen with the model bacterium, with over 90% cell

413   death detected in just 1 h of the NAg MIC exposure.[5] It is apparent that the elevated

414   cellular ROS generation has overwhelmed the naturally present anti-oxidant

415   mechanisms in the bacterium. The known presence of the superoxide dismutase

416   enzyme in the cytoplasm,[56] for example, seemed to be incapable to cope with the

417   nanoparticle-induced $O_2^{\bullet-}$ generation. Under normal condition, the ROS neutralizing

418   enzyme and peptide molecules maintain the cellular redox state within a safe threshold,

419   protecting the bacterium against oxygen radicals produced as by-products of aerobic

420   metabolism.[54] To the best of our knowledge however, no protein-based detoxification

421   systems have been identified in bacteria for the hydroxyl radical,[67] which is most likely

422   also a factor in the observed rapid killing of the model bacterium. Other types of cellular

423   reactive radicals that could also present in the NAg bacterial samples were the

424   hydroperoxyl ($HO_2^{\bullet-}$), a stronger oxidant than the superoxide,[49] as well as peroxynitrite

425   ($ONOO^-$). The latter rapidly forms when $O_2^{\bullet-}$ reacts with NO[54,65] (note that $ONOO^-$ is

426   also responsive to the CMH spin probing although at lesser interaction constant than

427     $O_2^{\bullet-}$ and $OH^{\bullet}$). The reactive nitrogen species can modify the amino acid tyrosine to

428   nitrotyrosine,[68] again, potentially affecting protein structures.[9]

429

430

431
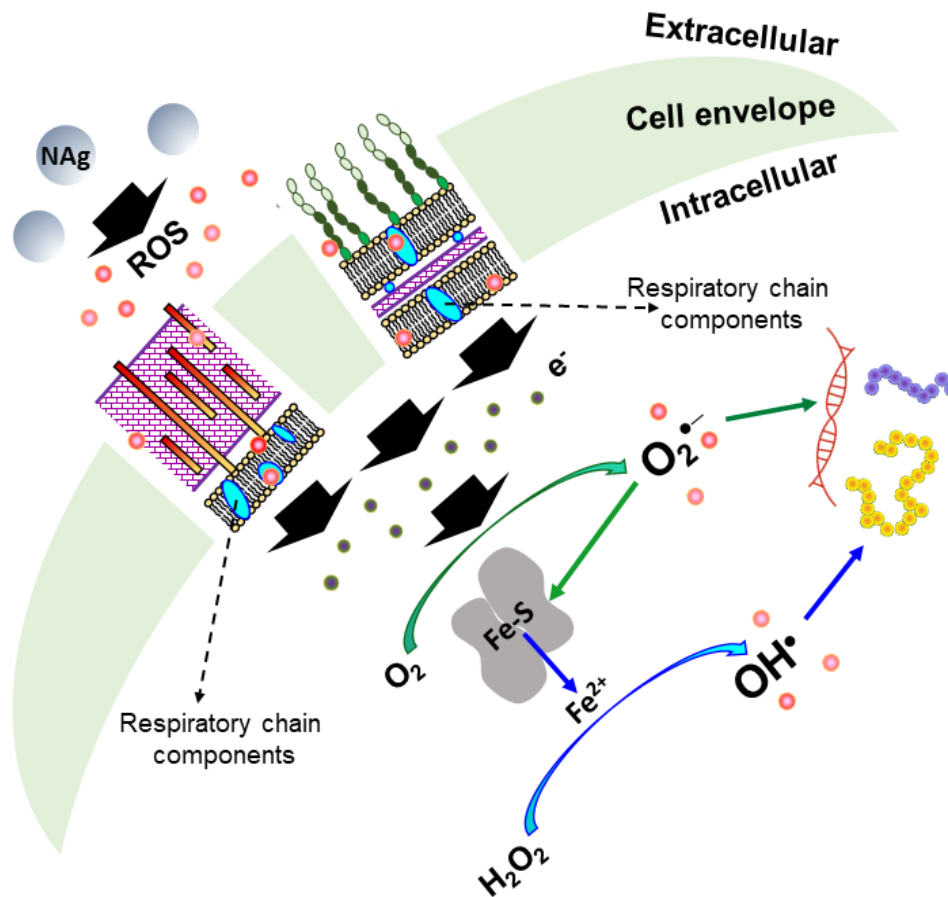
Scheme 2. **Antibacterial mechanisms of NAg: The link between cell envelope targeting and generation of oxygen radicals.** The work proposed an oxidative attack on the cell surface moieties – herein seen with the peptidoglycan, lipoteichoic acid as well as the membrane phospholipid, phosphatidylethanolamine, by reactive oxygen radicals, including those that are generated by the nanoparticle extracellularly, most likely during the leaching process. This intervenes with the activity of the membrane-bound respiratory chain components, causing leakage of electrons into the cytoplasm.[23,24,54,55] Molecular oxygen (O_2), due to its reduction potential, can readily capture these electrons, generating the herein detected superoxide radical ($O_2^{\bullet-}$) in the cells. The radical can destabilize iron-sulfur clusters in proteins, in turn, releasing the Fenton-active ferrous ions (Fe^{2+}) into the cytoplasm that leads to the observed generation of hydroxyl radical ($OH^{\bullet}$).[54,59,61,62] These radicals inflict oxidative damages on lipids, proteins and nucleic acids,[9,49,59] resulting in growth inhibition and cell death effects.[3,5]

446

CONCLUSIONS

This study examined the mechanisms of NAg toxicity on bacteria. Using ATR-FTIR spectroscopy, we showed that the nanoparticle inflicts major structural changes in the cell envelope components. NAg disintegrates the peptidoglycan, lipoteichoic acid and phosphatidylethanolamine (phospholipid) structures by disrupting their peptide and lipid chains as well as saccharide and phosphate groups. This damage is consistent with oxidative attacks, which could be imposed by the reactive oxygen radicals herein detected upon contact of the nanoparticle with aqueous systems. The cell envelope targeting, especially on the membrane phospholipid, is likely to subsequently trigger the observed generation of lethal levels of oxygen radicals, including the superoxide ($O_2^{\bullet-}$) and hydroxyl ($^{\bullet}OH$) radicals, in the cells (**Scheme 2**). This study concluded that ROS generation could be both the cause and consequence of NAg toxicity, being closely associated with the cell envelope targeting. Similar future work can also explore the influence of the nanoparticle's physicochemical characteristics – such as size, shape and presence of surface functional groups, as well as, equally important, the effects of silver-complexing and -precipitating agents – for example, the presence of halides (Cl^-, Br^-, I^-), amino acids and proteins in the environment and human tissues. With the now widespread use of NAg, an in-depth understanding of its toxicity modes is vital not only for the better assessment of the environmental and human health impact of the nanoparticle, but also for the urgent elucidation of the resistance phenomena. Recent studies have indeed revealed the ability of bacteria, including pathogens, to adapt and in turn, reduce the efficacy of the nanoparticle. The knowledge of how bacteria develop defence responses to the toxicity will contribute to the efforts to overcome the resistance effects.

EXPERIMENTAL SECTION

NAg effects on the bacterial cell envelope. The studies were performed by exposing isolated cell envelope components, the peptidoglycan (from *B. subtilis*, code 69554, Sigma-Aldrich), lipopolysaccharide (from *E. coli* 0111:B4, code L2630, Sigma-Aldrich), lipoteichoic acid (from *B. subtilis*, code L3265, Sigma-Aldrich) and phosphatidylethanolamine (from *E. coli*, Auspep), to NAg (finely dispersed flame-sprayed Ag, d_{TEM} = ~2 nm, on inert 30 nm TiO_2 support).[4] Each cell envelope component (2.0 mg L^{-1}) was exposed to NAg (0.12 mg Ag L^{-1} and 2.0 mg Ag L^{-1},

479 representing the lower and higher exposure dosages at 1:0.06 and 1:1 mass ratios,
480 respectively[28]) in water for 2 h at 37⁰C under dark condition. The latter is to avoid the
481 photocatalytic inactivation of the TiO_2 support.[4] Following exposure, the biomolecules
482 were lyophilised for water removal. Untreated biomolecules and biomolecules
483 incubated in water (no silver) were used as controls. The ATR-FTIR spectra (Nicolet
484 6700) were acquired by performing 64 scans (with 4 cm^{-1} spectral resolution) for each
485 sample. The spectra of only NAg were subtracted from those of the exposed cell
486 envelope components.

487 **ROS generation studies.** EPR enables detection of oxygen radicals based on
488 the absorption of electromagnetic radiation by the unpaired electrons that are present
489 in the free radicals when under magnetic field.[69] The ROS-sensitive cyclic
490 hydroxylamine 1-hydroxy3-methoxycarbonyl-2,2,5,5-tetramethylpyrrolidine (CMH) was
491 used as the spin probe. CMH reacts with the highest interaction constant with
492 superoxide radical ($O_2^{\bullet-}$). It is also responsive to hydroxyl radical (OH $^{\bullet}$), peroxynitrite
493 ($ONOO^-$), as well as peroxyl radicals (*e.g.* $HO_2^{\bullet-}$).[20,21] The signal intensity is directly
494 proportional to the ROS concentration in the sample.[70]

495 The studies were carried out on: (1) The NAg-only system in the absence of cells
496 for the detection of abiotically generated ROS, (2) the cell-only system, with no added
497 silver, for physiological cellular ROS detection, and (3) the NAg-cell system for the
498 nanoparticle-induced cellular ROS generation. For the NAg-only system, replicate
499 samples were prepared by aseptically adding pre-weighed NAg into 55 mL Luria
500 Bertani (LB) culture medium (10 mg L^{-1} NAg). To prepare the cell inoculum, a single
501 colony of *Bacillus subtilis* was cultured overnight at 30°C, 220 rpm in LB broth. A
502 volume of 1-3 mL of the overnight culture was then transferred into 50 mL fresh LB
503 broth for a further 0.5-1 h culturing (conditioning) at 37°C, 280 rpm. For the cell-only
504 system, replicate samples were prepared by aseptically adding 5 mL of the bacterial
505 inoculum into 50 mL LB broth (OD_{600} bacteria initial = 0.04, corresponding to ~2 x 10^7
506 cfu mL^{-1}). For the NAg-cell systems, replicate samples were prepared by aseptically
507 adding pre-weighed NAg into 55 mL of the bacterial culture (5 mL inoculum and 50 mL
508 broth, initial bacteria OD 0.04). Note that the NAg concentration was also 10 mg L^{-1},
509 the minimum inhibitory concentration of NAg on *B. subtilis*.[3,5] All systems were
510 incubated for 5 min, at 37°C, 280 rpm in the dark. The NAg-cell samples were subjected

511   to a two-step centrifugation procedure, to first remove the particulates (500 rpm, 5 min,

512   21ºC), then at 5000g, 10 min, 21ºC for sedimentation of cells and subsequent culture

513   medium removal. The cell-only system was subjected to the second centrifugation step

514   only. The NAg-only system was subjected to the first centrifugation step only.

515   The samples were immediately treated with the spin probe for ROS EPR analysis,

516   as follows. Cell pellets were suspended in 1 mL ice cold EPR-Krebs HEPES buffer (pH

517   7.4, Noxygen Science Transfer & Diagnostics GmbH), into which CMH stock (in EPR-

518   Krebs HEPES buffer) was added to a final concentration of 200 µM and reacted for 15

519   min at room temperature. For the NAg-only system, the spin probe was added into 1

520   mL of the supernatant. Aliquots of 50 µl from each system were loaded into Bruker

521   EMX X-Band EPR spectrometer, the spectra were collected with the following settings:

522   Magnetic field-center field 3505 G, sweep width 200 G, sweep time 30 s, sample g-

523   factor 2, signal channel-receiver gain 30 dB, mod. Amp 1 G, number of scans 4, offset

524   0%; microwave-attenuation 20 dB, power 2 mW. digital filter-mode auto, number of

525   points 10. The resulting spectra were recorded using Xenon software (Bruker). To

526   validate for the generation of $O_2^{\bullet-}$ and $OH^\bullet$ radicals in the systems, superoxide

527   dismutase (SOD, an $O_2^{\bullet-}$ scavenger, Sigma Aldrich) and dimethyl thiourea (DMTU, an

528    $OH^\bullet$ scavenger, Sigma Aldrich) were independently added to the NAg-cell systems at

529   a final concentration of 400 U and 20 mM, respectively, followed by 15 min reaction

530   time at room temperature. The spin probe CMH was then added, as described earlier.

535   *Supporting Information Available:* ATR-FTIR spectra for independent replicate NAg

536   exposure experiments on peptidoglycan, lipopolysaccharide, lipoteichoic acid,

537   phosphatidylethanolamine, EPR spectra for independent replicate ROS generation

538   experiments in NAg-only, cell-only, NAg-cell systems.

539

540

541

REFERENCES AND NOTES

(1) Gunawan, C.; Marquis, C.P.; Sotiriou, G.A.; Rice, S.A.; Harry, E.J. Widespread and Indiscriminate Nanosilver Use: Genuine Potential for Microbial Resistance. *ACS Nano* **2017**, 11, 3438-3445.

(2) Prasath, S.; Palaniappan, K. Is Using Nanosilver Mattresses/Pillows Safe? A Review of Potential Health Implications of Silver Nanoparticles on Human Health. *Environ. Geochem. Health* **2019**, https://doi.org/10.1007/s10653-019-00240-7

(3) Faiz, M.B.; Amal, R.; Marquis, C.P.; Harry, E.J.; Sotiriou, G.A.; Rice, S.A.; Gunawan, C. Nanosilver and the Microbiological Activity of the Particulate Solids Versus the Leached Soluble Silver. *Nanotoxicology* **2018**, 12, 263-273.

(4) Gunawan, C.; Teoh, W.Y.; Marquis, C.P.; Lifia, J.; Amal, R. Reversible Antimicrobial Photoswitching in Nanosilver. *Small* **2009**, 5, 341–344.

(5) Gunawan, C.; Teoh, W.Y.; Marquis, C.P.; Amal, R. Induced Adaptation of *Bacillus* sp. to Antimicrobial Nanosilver. *Small* **2013**, 21, 3554-3560.

(6) Sotiriou, G.A.; Pratsinis, S.E. Antibacterial Activity of Nanosilver Ions and Particles. *Environ. Sci. Technol.* **2010**, 44, 5649-5654.

(7) Hansen, S.F.; Baun, A. When Enough is Enough. *Nat. Nanotechnol.* **2012**, 7, 409-411.

(8) Faunce, T.; Watal, A. Nanosilver and Global Public Health: International Regulatory Issues. *Nanomedicine* **2010**, 5, 617-632.

(9) Ezraty, B.; Gennaris, A.; Barras, F.; Collet, J.F. Oxidative Stress, Protein Damage and Repair in Bacteria. *Nat. Rev. Microbiol.* **2017**, 15, 385-396.

(10) Cabiscol, E.; Tamarit, J.; Ros, J. Oxidative Stress in Bacteria and Protein Damage by Reactive Oxygen Species. *Internatl. Microbiol.* **2000**, 3, 3-8.

(11) Abbas, H.; Maikhuri, D.; Sharma, C. Interaction and Damage of Nucleobases of DNA and RNA Caused by Silicon Nanoparticle and Crystalline Silica: First Principles Study. *Comput. Theor. Chem.* **2019**, 1154, 26-30.

(12) Nimse, S.B.; Pal, D. Free Radicals, Natural Antioxidants, and their Reaction Mechanisms. *RSC Adv.* **2015**, 5, 27986-28006.

571 (13) Ramalingam, B.; Parandhaman, T.; Das, S.K. Antibacterial Effects of
572   Biosynthesized Silver Nanoparticles on Surface Ultrastructure and Nanomechanical
573   Properties of Gram-Negative Bacteria viz. *Escherichia coli* And *Pseudomonas*
574   *aeruginosa. ACS Applied Materials & Interfaces* **2016**, 8, 4963-4976.

575 (14) Sondi, I.; and Salopek-Sondi, B. Silver Nanoparticles as Antimicrobial Agent: A
576   Case Study on *E. coli* as a Model for Gram-Negative Bacteria. *Journal of Colloid*
577   *and Interface Science* **2004**, 75, 177-182.

578 (15) Maillard, A.P.V.F.; Gonçalves, S.; Santos, N.C.; Mishima, B.A.L.D.; Dalmasso,
579   P.R.; Hollmann, A. Studies on Interaction of Green Silver Nanoparticles with Whole
580   Bacteria by Surface Characterization Techniques. *BBA-Biomembranes* **2019**, 1861,
581   1086-1092.

582 (16) Kiwi, J.; Nadtochenko, V. Evidence for the Mechanism of Photocatalytic
583   Degradation of the Bacterial Wall Membrane at the TiO_2 Interface by ATR-FTIR and
584   Laser Kinetic Spectroscopy. *Langmuir* **2005,** 21, 4631-4641.

585 (17) Fels, L.E.; Zamama, M.; Hafidi, M. Advantages and Limitations of Using FTIR
586   Spectroscopy for Assessing the Maturity of Sewage Sludge and Olive Oil Waste
587   Co-Composts. In *Biodegradation and bioremediation of polluted systems – New*
588   *advances and technologies;* Intech Open Science: 2015; pp 127-144.

589 (18) Sharma, P.; Jha, A.B.; Dubey, R.S.; Pessarakli, M. Reactive Oxygen Species,
590   Oxidative Damage, and Antioxidative Defense Mechanism in Plants under Stressful
591   Conditions. *Journal of Botany* **2012**, 217037, 1-26.

592 (19) Das, K.; Roychoudhury, A. Reactive Oxygen Species (ROS) and Response of
593   Antioxidants as ROS-Scavengers during Environmental Stress in Plants. *Frontiers*
594   *in Environmental Science* **2014**, 2, 1-13.

595 (20) Gielis, J.F.; Boulet, G.A.; Briedé, J.J.; Horemans, T.; Debergh, T.; Kussé, M.; Cos,
596   P.; Van Schil, P.E. Longitudinal Quantification of Radical Bursts during Pulmonary
597   Ischaemia and Reperfusion. *Eur J Cardiothorac. Surg* **2015**, 48, 622-629.

598 (21) Thomas, V.C.; Chaudhari, S.S.; Jones, J.; Zimmerman, M.C.; Bayles, K.W. Electron
599   Paramagnetic Resonance (EPR) Spectroscopy to Detect Reactive Oxygen Species
600   in *Staphylococcus aureus*." *Bio Protoc.* **2015**, 5, e1586.

601   (22) Mirzajani, F.; Ghassempour, A.; Aliahmadi, A.; Esmaeili, M.A. Antibacterial Effect
602   of Silver Nanoparticles on *Staphylococcus aureus*. *Research in Microbiology* **2011**,
603   162, 542-549.

604   (23) Li, W.R.; Xie, X.B.; Shi, Q.S.; Zeng, H.Y.; Yang, Y.S.O.U.; Chen, Y.B. Antibacterial
605   Activity and Mechanism of Silver Nanoparticles on *Escherichia coli*. *Applied*
606   *Microbiology and Biotechnology* **2010,** 85, 1115-1122.

607   (24) Li, W.R.; Xie, X.B.; Shi, Q.S.; Duan, S.S.; Ouyang, Y.S.; Chen, Y.B. Antibacterial
608   Effect of Silver Nanoparticles on *Staphylococcus aureus*. *BioMetals* **2011,** 24, 135-
609   141.

610   (25) Auer, G.K.; Weibel, D.B. Bacterial Cell Mechanics. *Biochemistry* **2017**, 56, 3710-
611   3724.

612   (26) Irazoki, O.; Hernandez, S.B.; Cava F. Peptidoglycan Muropeptides: Release,
613   Perception, and Functions as Signaling Molecules. *Frontiers in Microbiology* **2019**,
614   10, 1-17.

615   (27) Morè N.; Martorana, A.M.; Biboy, J.; Otten, C.; Winkle, M.; Serrano, C.K.G.; Silva,
616   A.M.; Atkinson, L.; Yau, H.; Breukink, E.; Blaauwen, T.D.; Vollmer, W.; Polissi, A.
617   Peptidoglycan Remodelling Enables *Escherichia coli* to Survive Severe Outer
618   Membrane Assembly Defect. *mBio* **2019**, 10, e02729-18.

619   (28) Jiang, W.K.; Yang, K.; Vachet, R.W.; Xing, B. Interaction between Oxide
620   Nanoparticles and Biomolecules of the Bacterial Cell Envelope as Examined by
621   Infrared Spectroscopy. *Langmuir* **2010**, 26, 18071–18077.

622   (29) Madigan, M.T.; Martinko, J.M.; Stahl, D.A.; Clark, D.P. *Brock Biology of*
623   *Microorganisms* (13th Edition); Benjamin Cummings, **2012.**

624   (30) Ansari, M.A.; Khan, H.M.; Khan, A.A.; Ahmad, M.K.; Mahdi, A.A.; Pal, R.; Cameotra,
625   S.S. Interaction of Silver Nanoparticles with *Escherichia coli* and their Cell Envelope
626   Biomolecules. *J. Basic Microbiol.* **2014**, 54, 905–915.

627   (31) Naumann, D.; Barnickel, G.; Bradaczek, H.; Labischinski, H.; Giesbrecht, P. Infrared
628   Spectroscopy, a Tool for Probing Bacterial Peptidoglycan. Potentialities of Infrared

629   Spectroscopy for Cell Wall Analytical Studies and Rejection of Models based on
630   Crystalline Chitin. *Eur J Biochem* **1982**, 125, 505-515.

631 (32) Kačuráková, M.; Mathlouthi, M. FTIR and Laser-Raman Spectra of
632   Oligosaccharides in Water: Characterization of the Glycosidic Bond. *Carbohydrate*
633   *Research* **1996**, 284, 145-157.

634 (33) Naumann, D. Infrared Spectroscopy in Microbiology. In *Encyclopedia of Analytical*
635   *Chemistry;* Meyers, R.A., Eds.; John Wiley & Sons Ltd: Chichester, **2000**, pp 102–
636   131.

637 (34) Naumann, D.; Schultz, C.; Born, J.; Labischinski, H.; Brandenburg, K.; Von Busse,
638   G.; Brade, H.; Seydel, U. Investigations into the Polymorphism of Lipid A from
639   Lipopolysaccharides of *Escherichia coli* And *Salmonella minnesota* by Fourier-
640   Transform Infrared Spectroscopy. *European Journal of Biochemistry* **1987**, 164,
641   159-169.

642 (35) Jucker, B.A.; Harms, H.; Hug, S.J.; Zehnder, A.J.B. Adsorption of Bacterial Surface
643   Polysaccharides on Mineral Oxides is Mediated by Hydrogen Bonds." *Colloids and*
644   *Surfaces B: Biointerfaces* **1997**, 9, 331-343.

645 (36) Parikh, S.J.; Chorover, J. ATR-FTIR Study of Lipopolysaccharides at Mineral
646   Surfaces. *Colloids and Surfaces B: Biointerfaces* **2008**, 62, 188–198.

647 (37) Neu, T.R.; Marshall, K.C. Bacterial Polymers: Physicochemical Aspects of their
648   Interactions at Interfaces. *Journal of Biomaterial Applications* **1990**, 5, 107-133.

649 (38) Omoike, A.; Chorover, J. Spectroscopy Study of Extracellular Polymeric
650   Substances from *Bacillus subtilis*: Aqueous Chemistry and Adsorption Effects.
651   *Biomacromolecules* **2004**, 5, 1219-1230.

652 (39) Schneewind, O.; Missiakas, D. Lipotechoic Acids, Phosphate-Containing Polymers
653   in the Envelope of Gram-Positive Bacteria. *Journal of Bacteriology* **2014**, 196, 1133-
654   1142.

655 (40) Hsueh, Y.H.; Lin, K.S.; Ke, W.J.; Hsieh, C.T.; Chiang, C.L.; Tzou, D.Y.; Liu, S.T.
656   The Antimicrobial Properties of Silver Nanoparticles in *Bacillus subtilis* are Mediated
657   by Released Ag^+ Ions. *PLoS one* **2015**, 12, e144306.

658 (41) Amro, N.A.; Kotra, L.P.; Wadu-Mesthrige, K.; Bulychev, A.; Mobashery, S.; Liu, G.Y.
659   High-Resolution Atomic Force Microscopy Studies of the *Escherichia coli* Outer
660   Membrane: Structural Basis for Permeability. *Langmuir* 2000, **16**, 2789-2796.

661 (42) Kim, J.S.; Kuk, E.; Yu, K.N.; Kim, J.H.; Park, S.J.; Lee, H.J.; Kim, S.H.; Park, Y.K.;
662   Park, Y.H.; Hwang, C.Y.; Kim, Y.K.; Lee, Y.S.; Jeong, D.H.; Cho, M.H. Antimicrobial
663   Effects of Silver Nanoparticles. *Nanomedicine* **2007**, 3, 95-101.

664 (43) Choi, O., Deng, K.K.; Kim, N.J.; Ross Jr, L.; Surampalli, R.Y.; Hu, Z. The Inhibitory
665   Effects of Silver Nanoparticles, Silver Ions, and Silver Chloride Colloids on Microbial
666   Growth. *Water Research* **2008**, 42, 3066-3074.

667 (44) Berg, K.; Ericsson, M.; Lindgren, M.; Gustafsson, H.K. A High Precision Method for
668   Quantitative Measurements of Reactive Oxygen Species in Frozen Biopsies." *PLoS*
669   *One* **2014**, 9,e90964.

670 (45) Liu, J.; Hurt, R.H. Ion Release Kinetics and Particle Persistence in Aqueous Nano-
671   Silver Colloids. *Environmental Science & Technology* **2010**, 44, 2169–2175.

672 (46) Molleman, B.; Hiemstra, T. Surface Structure of Silver Nanoparticles as a Model for
673   Understanding the Oxidative Dissolution of Silver Ions. *Langmuir* **2015**, 31,
674   13361−13372.

675 (47) Paria, S.; Halder, P.; Paine, T.K. Oxidative Carbon-Carbon Bond Cleavage of a α-
676   Hydroxy Ketone by a Functional Model of 2,4'-Dihydroxyacetophenone
677   Dioxygenase. *Angew. Chem. Int. Ed.* **2012**, 51, 6195-6199.

678 (48) Zhang, Y.; Sugai, T.; Yamamoto, T.; Yamamoto, N.; Kutsumura, N.; Einaga, Y.;
679   Nishiyama, S.; Saitoh, T.; Nagase, H. Oxidative Cleavage of the Acyl-Carbon Bond
680   in Phenylacetone with Electrogenerated Superoxide Anions. *ChemElectroChem*
681   **2018**, 5, 1-6.

682 (49) Ayala, A.; Muñoz, M.F.; Argüelles, S. Lipid Peroxidation: Production, Metabolism,
683   and Signalling Mechanisms of Malondialdehyde and 4-Hydroxy-2-Noenal.
684   *Oxidative Medicine and Cellular Longevity* **2014**, 360438, 1-31.
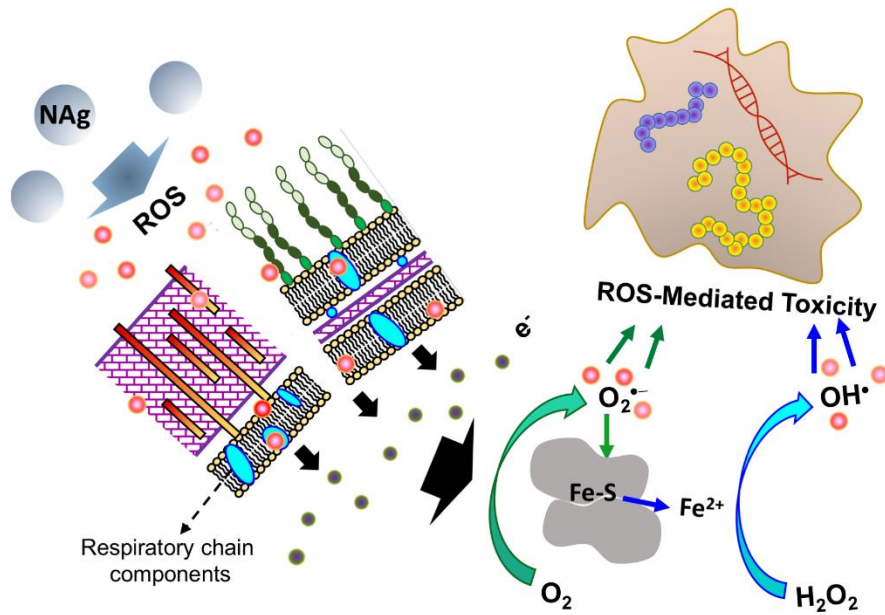
685   (50) Mahmoud, M.A.M..; El-Demerdash, S.H.; Gogary, T.M.E.L.; El-Nahas, A.M.
686   Oxidation of Methyl Propanoate by the OH Radical. *Russian Journal of Physical*
687   *Chemistry* **2018**, 92, 2476-2484.

688   (51) Hayon, E.; Ibata, T.; Lichtin, N.N.; Simic, M. Sites of Attack of Hydroxyl Radicals on
689   Amides in Aqueous Solution. *Journal of the American Chemical Society* **1971**, 93,
690   5388-5394.

691   (52) Samuni, A.; Neta, P. Hydroxyl Radical Reaction with Phosphate Esters and the
692   Mechanims of Phosphate Cleavage. *The Journal of Physical Chemistry* **1973**, 77,
693   2425-2429.

694   (53)   Morones, J.R.; Elechiguerra, J.L.; Camacho, A.; Holt, K.; Kouri, J.B.; Ramírez,
695   J.T.; Yacaman, M.J. The Bactericidal Effect of Silver Nanoparticles.
696   *Nanotechnology* **2005**, 16, 2346-2353.

697   (54) Mols, M.; Abee, T. Primary and Secondary Oxidative Stress in *Bacillus*. *Environ*
698   *Microbiol* **2011**, 13, 1387-1394.

699   (55) Holt, K.B.; Bard, A.J. Interaction of Silver(I) Ions with the Respiratory Chain of
700   *Escherichia coli*: An Electrochemical and Scanning Electrochemical Microscopy
701   Study of the Antimicrobial Mechanism of Micromolar Ag^+. *Biochemistry* **2011**, 44,
702   13214-13223.

703   (56) Imlay, J.A. Cellular Defenses Against Superoxide and Hydrogen Peroxide. *Annu*
704   *Rev Biochem* **2008**, **77**: 755–776.

705   (57) Hwang, E.T.; Lee, J.H.; Chae, Y.J.; Kim, Y.S.; Kim, B.C.; Sang, B.I.; Gu, M.B.
706   Analysis of the Toxic Mode of Action of Silver Nanoparticles using Stress-Specific
707   Bioluminescent Bacteria. *Small* **2008**, 4, 746-750.

708   (58) Dwyer, D.J.; Kohanski, M.A.; Collins, J.J. Role of Reactive Oxygen Species in
709   Antibiotic Action and Resistance. *Curr Opin Microbiol* **2009**, 12, 482-489.

710   (59) Lemire, J.A.; Harrison, J.J.; Turner, R.J. Antimicrobial Activity of Metals:
711   Mechanisms, Molecular Targets and Applications. *Nat Rev Micro* **2013**, 11, 371-
712   384.

713 (60) Vernis, L.; Banna, N.E.; Baïlle, D.; Hatem, E.; Heneman, A.; Huang, M.E. Fe-S
714   Clusters Emerging as Targets of Therapeutic Drugs. *Oxidative Medicine and*
715   *Cellular Longevity* **2017**, 3647657, 1-12.

716 (61) Macomber, L.; Imlay, J.A. The Iron-Sulfur Clusters of Dehydratases are Primary
717   Intracellular Targets of Copper Toxicity. *Proc Natl Acad Sci U S A* **2009**, 106, 8344-
718   8349.

719 (62) Imlay, J.A. Pathways of Oxidative Damage. *Annu. Rev. Microbiol.* **2003**, 57, 395–
720   418.

721 (63) Gordon, O., Vig Slenters, T.; Brunetto, P.S.; Villaruz, A.E.; Sturdevant, D.E.; Otto,
722   M.; Landmann, R.; Fromm, K.M. Silver Coordination Polymers for Prevention of
723   Implant Infection: Thiol Interaction, Impact on Respiratory Chain Enzymes, and
724   Hydroxyl Radical Induction. *Antimicrobial Agents and Chemotherapy* **2010**, 54,
725   4208-4218.

726 (64) Yin, H.; Xu, L.; Porter, N.A. Free Radical Lipid Peroxidation: Mechanisms and
727   Analysis. *Chemical Reviews* **2011**, 111, 5944-5972.

728 (65) D'Autreaux, B.; Toledano, M.B. ROS as Signalling Molecules: Mechanisms that
729   Generate Specificity in ROS Homeostasis. *Nat Rev Mol Cell Biol* **2007**, 8, 813-824.

730 (66) Kohanski, M.A.; Dwyer, D.J.; Hayete, B.; Lawrence, C.A.; Collins, J.J. A Common
731   Mechanism of Cellular Death Induced by Bactericidal Antibiotics. *Cell* **2007**, 130,
732   797-810.

733 (67) Zhao, X.; Drlica, K. Reactive Oxygen Species and the Bacterial Response to Lethal
734   Stress. *Curr. Opin. Microbiol.* **2014**, 21, 1-6.

735 (68) Sawa, T.; Akaike, T.; Maeda, H. Tyrosine Nitration by Peroxynitrite Formed from
736   Nitric Oxide and Superoxide Generated by Xanthine Oxidase. *The Journal of*
737   *Biological Chemistry* **2000**, 275, 32467-32474.

738 (69) He, W.; Liu, Y.; Wamer, W.G.; Yin, J.J. Electron Spin Resonance Spectroscopy for
739   the Study of Nanomaterial-Mediated Generation of Reactive Oxygen Species.
740   *Journal of Food and Drug Analysis* **2014**, 22, 49-63.

741 (70) Acker, H.V.; Gielis, J.; Acke, M.; Cools, F.; Cos, P.; Coenye, T. The Role of Reactive

742   Oxygen Species in Antibiotic-Induced Cell Death in *Burkholderia cepacia* Complex

743   Bacteria. *PLoS One* **2016**, 11, e0159837.

744

745 **Table of Contents Graphic**

746